ARTICLE

Plugging into Proteins: Poisoning Protein Function by a Hydrophobic Nanoparticle

Guanghong Zuo,[†,‡] Qing Huang,[‡] Guanghong Wei,[†] Ruhong Zhou,[§,⊥,*] and Haiping Fang[†,‡,*]

[†]T-Life Research Center, Department of Physics, Fudan University, Shanghai 200433, China, [‡]Shanghai Institute of Applied Physics, Chinese Academy of Sciences, P.O. Box 800-204, Shanghai 201800, China, [§]IBM Thomas J. Watson Research Center, Yorktown Heights, New York 10598, United States, and [⊥]Department of Chemistry, Columbia University, New York, New York 10027, United States

ABSTRACT Nanoscale particles have become promising materials in many fields, such as cancer therapeutics, diagnosis, imaging, drug delivery, catalysis, as well as biosensors. In order to stimulate and facilitate these applications, there is an urgent need for the understanding of the nanoparticle toxicity and other risks involved with these nanoparticles to human health. In this study, we use large-scale molecular dynamics simulations to study the interaction between several proteins (WW domains) and carbon nanotubes (one form of hydrophobic nanoparticles). We have found that the carbon nanotube can plug into the hydrophobic core of proteins to form stable complexes. This plugging of nanotubes disrupts and blocks the active sites of WW domains from binding to the corresponding ligands, thus leading to the loss of the original function of the proteins. The key to this observation is the hydrophobic interaction between the nanoparticle and the hydrophobic residues, particularly tryptophans, in the core of the domain. We believe that these findings might provide a novel route to the nanoparticle toxicity on the molecular level for the hydrophobic nanoparticles.

KEYWORDS: nanoparticle toxicity · protein−nanoparticle interaction · protein function poisoning · hydrophobic interaction · molecular dynamics

Nanoparticles are highly promising candidates for various important biological applications, such as gene delivery,[1] cellular imaging,[2] tumor therapy,[3] and biological experimental technology.[4] Meanwhile, the interaction between nanoparticles and the biological systems has received great attention since this may bring some biosafety concerns.[5−10] Recent experiments have shown that unrefined single-wall carbon nanotubes (SWCNTs) might be aerosolized and release fine particles into the air.[11] When the concentration of multiwall carbon nanotubes (MWCNTs) in air is sufficiently high, they can be inhaled and then migrate in body.[12] These carbon nanotubes, both SWCNTs and MWCNTs, can enter cells and accumulate in cytoplasms,[13,14] which may lead to the lung insult,[15−18] immunologic toxicity,[19] and adverse cardiovascular effects[20] on mammals, including human beings. Proteins are the functional units of life. Studies on the interaction of the nanoparticles and proteins may provide a key to understand the basic questions in nanotoxicology and nanopharmacology.

There is an increasing interest in the interactions between nanoparticles and proteins in recent years.[21−26] Most of these studies so far focus on the nanoparticle−protein corona formed by the absorption of the proteins on the surface of the nanoparticle.[21−23] For example, a recent molecular dynamics simulation shows that the conformation of a subdomain of human serum albumin can be significantly affected by its absorption onto carbon nanotube surfaces.[24] Separately, it is also shown that some small peptides, such as collagen-like peptides, can be encapsulated in large nanotubes, even though their conformations are barely affected.[27] We note, in 2003, Park *et al.* showed experimentally that, with suitable sizes and shapes, the SWCNTs are effective in blocking some biological membrane ion channels.[28] Calvaresi and Zerbetto also found that proteins interacting with C_{60} generally have good shape matches with C_{60} through their docking studies.[29] Despite these studies, the mechanism, particularly, the effect of nanoparticles on the structure and function of biomolecules, which may lead to the loss of the original function of the proteins, is far from being understood. Various experimental techniques have been developed to shed light onto this important problem; however, the inherent difficulties involved in these complex settings can limit their applications due to too many other factors involved ("side effects"), and results may vary even with the same nanoparticles with the same chemical composition (same shape, length, and aggregation property, *etc.*). The computational simulations, on the other hand, might be able to mimic these

*Address correspondence to ruhongz@us.ibm.com, fanghaiping@sinap.ac.cn.

Received for review July 26, 2010 and accepted November 8, 2010.

Published online November 16, 2010. 10.1021/nn101762b

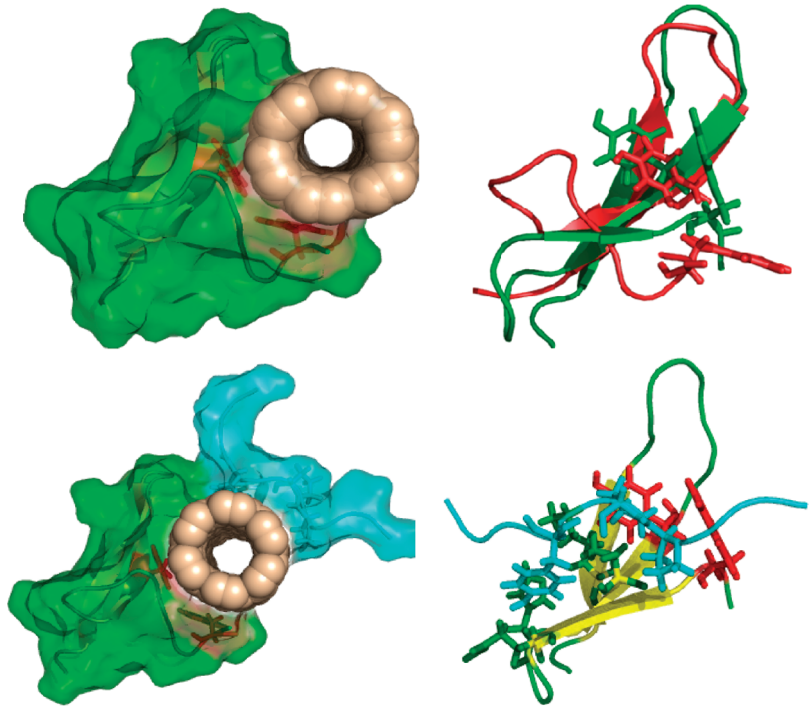

Figure 1. Typical structures of (top left) a complex of the YAP65WW protein domain and the single-walled carbon nanotube (SWCNT) showing the insertion of the SWCNT into the protein domain. WW domain (top right) in the complex (red) superposed with its native state (green). Protein−SWCNT complex (bottom left) with the adsorbed proline-rich motif (PRM), and (bottom right) domain binding with the PRM (PDB code 1JMQ). Here, the YAP65WW protein domain is shown as a cartoon with a yellow strand and green loop, and the key residues (W39 and Y28) are identified by red sticks. The (6,6) armchair SWCNT has a diameter of 8.08 Å, and its atoms are shown as wheat spheres. The PRM with the sequence GTPPPPYTVG, which binds the YAP65WW domain, is shown as cyan cartoons with the key residues identified by sticks. The solvated surfaces are shown for the complex.

kinds of interactions and avoid some complicated side effects. Here we show that a SWCNT, one form of nanoparticle, can plug into the hydrophobic core of a protein to form a stable complex, leading to potential poisoning of the protein function by disrupting and blocking its active site. One key to this observation is the small size of the SWCNT, which can be inserted into the hydrophobic core of the protein instead of the more common adsorption of proteins onto nanoparticle surfaces.[21−24]

We take the WW domains (YAP65, YJQ8, and PIN1) and the SWCNTs as examples to illustrate the idea. The WW domains are signaling and regulatory proteins used as functional modules to identify and bind to the proline-rich motifs (PRMs). They exist as a triple stranded antiparallel β-sheet structure.[30] The SWCNTs,[31,32] on the other hand, are widely used in many applications in bio- and nanotechnologies. We have found that a SWCNT can plug into the hydrophobic core of WW domains to form stable complexes due to favorable interactions with hydrophobic residues.

RESULTS AND DISCUSSION

The molecular configuration in our arrangement consists of a WW domain (*e.g.*, YAP65WW domain,[30] the human Yes-associated protein) and an armchair SWCNT with various sizes. The SWCNT and protein were initially well-separated, with a distance between the geometric center of protein domain and the SWCNT of 15.0 Å and the minimum distance of more than 8.3 Å. Each system was solvated with the TIP3P model water. The solvated systems were then simulated with molecular dynamics (MD), which have been widely used in studies of biomolecules[33−49] and nanoscale systems.[50−54] Here, we performed 36 independent simulations for the YAP65WW domain and various sizes of SWCNTs with different initial velocities, each with 200 ns. Additional simulations with other WW domains, including YJQ8 and PIN1, and various sizes of SWCNTs were further performed to obtain another 200 trajectories (see details in the Supporting Information).

We found several cases in our simulations that the SWCNTs plugged into the YAP65WW domain between the second and third β-strands, as shown in Figure 1. This is in contrast to the conventional idea that it is generally difficult to bring the carbon nanotubes into protein interiors because proteins in general have well-defined three-dimensional structures with a "protective" hydrophilic surface layer. From Figure 1, we can see the main change of the protein conformation in the complex is in its third β-strand, which unfolds into a loop and then wraps on the SWCNT, with most of its contacts with the second β-strand broken. In essence, these conformational changes are prere-

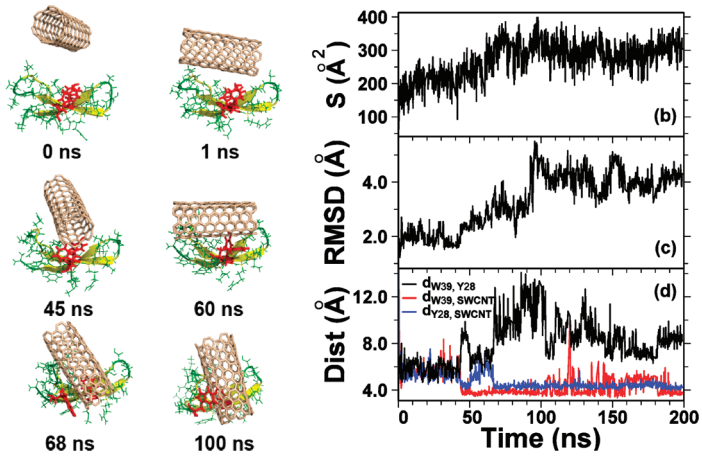

Figure 2. Typical trajectory of the YAP65WW domain together with a SWCNT. Left: Representative snapshots at various times. The proteins are shown as cartoons with yellow β-strands and green loops. The binding scaffold residues are noted by red sticks, and the SWCNTs are shown as wheat sticks. (b) Interface area of the WW domain and the SWCNT. (c) Root mean square deviation (rmsd) of the YAP65WW domain from its native structure, and (d) distances between the SWCNT and the key residues of YAP65WW domain, W39 (red), and Y28 (blue), and distance between these two residues (black), denoted by $d_{W39,Y28}$, $d_{W39,SWCNT}$, and $d_{Y28,SWCNT}$, respectively, as a function of time.

quirements for the formation of this complex of the protein domain and the SWCNT. There are nine residues in the second and third β-strands that bind to the SWCNT, with most of them hydrophobic residues such as Trp39 (more below). Thus, we believe that the hydrophobic interaction, the dominant force for protein folding,[55] is the key to this phenomenon, in which the SWCNT plugs into the core of the WW protein domain to form a stable protein−SWCNT complex.

Figure 2 displays some representative snapshots of this complex at different times to show how the SWCNT plugs into the protein domain. We used the interface area between the protein domain and the SWCNT (denoted by S, shown in Figure 2b) to illustrate this process. Here S is defined as half of the difference between the solvent-accessible surface area of the complex and the sum of solvent-accessible surface areas of the protein and the SWCNT. At $t = 0$, the center of protein domain and the SWCNT is 15.0 Å apart and S is small (~50 Å^2). S rises to about 200 Å^2 within 1 ns, showing that the protein domain and the SWCNT approached each other very quickly. As can also be seen from Figure 2, the SWCNT was absorbed onto the protein surface at $t = 1$ ns. S gradually increased from ~200 to ~250 Å^2 in the first 45 ns, with significant fluctuations along the way. From the movie shown in Supporting Information, we found that, while the SWCNT was being absorbed onto the WW domain surface, the contacting surface region of the domain kept changing, which indicates that the SWCNT was constantly seeking a more stable binding site. Around $t = 45$ ns, there was a negative impulse in the interface area S. A careful examination showed that the SWCNT began to plug into the second and the third β-strands, and the negative impulse was a result of the opening of the second and the third β-strands before the SWCNT was "swallowed" by the protein. S reached its maximal value of ~300 Å^2 at $t =$ ~80 ns, meaning that the SWCNT was finally successful in plugging into the protein domain. We found that the SWCNT was basically wrapped by the second and the third β-strands, forming a complex of the WW domain with the SWCNT. From $t = 80$ ns up to 200 ns, there were only minor fluctuations of S at ~300 Å^2, showing the stability of this protein−SWCNT complex.

We have computed the rmsd of the YAP65WW domain from its native structure (Figure 2c). There are three major "steps" in the rmsd. At the first step, the rmsd was maintained at roughly 2.0 Å before $t = 45$ ns. During this time period, the SWCNT was absorbed onto the protein surface but had only limited impact on the conformation of the protein. In the second step, from time interval of ~45 to ~70 ns, the rmsd increased gradually from ~2.0 to ~3.5 Å, corresponding to the opening of the second and third β-strands due to the insertion of the SWCNT. Interestingly, from ~70 to 100 ns, a small plateau in the rmsd, around 3.0 Å, appeared, which was due to the partial recovery of the contacts between the second and third β-strand. Around 100 ns, there is a significant jump in the rmsd, from 3.0 to 4.0 Å, marked by its third step. During this jump, we found that there is a change in both the orientation and binding site of the indole ring of W39 residue on the SWCNT. From $t = 100$ ns, the rmsd was roughly constant at ~4.0 Å, indicating that the final complex of the WW domain and SWCNT was quite stable. For comparison, we have also performed simulations for the WW domain only (without any SWCNT and ligand) and found that the rmsd of the WW domain remained at a value of around 2.0 Å (see Figure S1). Thus, this significant conformational alteration of the YAP65WW domain is caused by the interaction and insertion of the SWCNT.

There exist two highly conserved residues, a tryptophan residue in the third β-strand and an aromatic residue in the second β-strand, either tryptophan or tyrosine, in the WW domain, which are critical for its function.[30] For the YAP65WW domain, these two key residues are W39 and Y28, respectively. In Figure 2d, we show the distance between these two residues and distances between each residue with the SWCNT as a function of time, denoted by $d_{W39,Y28}$, $d_{W39,SWCNT}$, and $d_{Y28,SWCNT}$, respectively. Before $t = 45$ ns, $d_{W39,Y28}$, $d_{W39,SWCNT}$, and $d_{Y28,SWCNT}$ were all kept almost as a constant at ~6.0 Å with small fluctuations, showing that the two key residues were "confined" at their native state, and the initial adsorption of the SWCNT does not impact much on their structures and orientations. In the period of $t = 45-55$ ns, there was an impulse jump in $d_{W39,Y28}$ to a value around 9 Å and a drop in $d_{Y28,SWCNT}$ to a valley around 4 Å. These changes indicate the detachment of W39 with Y28 and the approach of Y28 to the SWCNT. At the same time, $d_{W39,SWCNT}$ decreased sharply to <4 Å and remained there for the rest of the simulations, which indicates a strong and favorable in-

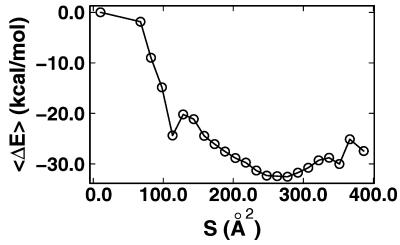

Figure 3. Interaction potential energy of the system as a function of interface area *S* of the YAP65WW domain and a (6,6) SWCNT, averaged from six trajectories of the complex.

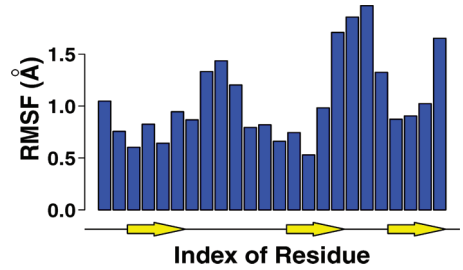

Figure 4. Root mean square fluctuation of the non-hydrogen atoms for the simulation of the YAP65WW domain without SWCNT. The yellow arrows show the three β-strands of the WW domain. The secondary structure information of the domain is obtained by DSSP.[58]

teraction between W39 and the SWCNT. It is interesting to note that this favorable tryptophan−CNT interaction has also been observed in recent phage display experiments for CNT−peptide interactions (adsorption of peptides onto CNT).[56,57] Therefore, even though we do not have direct experimental evidence at this point for this plugging of SWCNTs, it might not be totally impossible due to the strong and favorable interactions between CNTs and hydrophobic residues with aromatic rings such as tryptophans. At $t = 55-70$ ns, both $d_{Y28,W39}$ and $d_{Y28,SWCNT}$ returned to their values before $t = 45$ ns. By careful examination of the trajectory movie, we found that there was a rotation of the orientation of the SWCNT with the SWCNT firmly seizing the W39. After $t = 70$ ns, $d_{Y28,SWCNT}$ decreased to a small value again (~4 Å), and $d_{W39,\ Y28}$ turned to a significantly larger value (8−12 Å). This shows a significantly larger separation of the two active-site residues, corresponding to the completely opened second and third β-strands and a potential loss of protein function.

We have computed the interaction potential energy of the system as the function of the interface area between the YAP65WW domain and a (6,6) SWCNT. Figure 3 shows the results averaged from six trajectories of the complex. There is a basin at about $S = 280$ Å^2, with the interaction energy being about 30.0 kcal/mol less than the interaction energy of the state when the YAP65WW domain and the SWCNT are well-separated. As shown in Figure 2b, we can see that $S \sim 280$ Å^2 corresponds to the state in which a SWCNT plugs into the YAP65WW domain. That is, the complex of the WW domain and SWCNT is a more favored state in terms of the total interaction energy. The interface area with values larger than 280 Å^2 shown in Figure 3 results from the conformational fluctuations of the YAP65WW domain as shown in Figure 2b.

In addition to the YAP65WW−SWCNT complexes found in above simulations, many more such protein−SWCNT complexes have been observed with other WW domains and SWCNTs of various radii (see details in the Supporting Information). All of those systems have considerable increases in the interfacial area *S* and significant changes in the distances between the active sites and the SWCNT. In contrast, for the cases where only the mere absorptions of SWCNTs happen on the WW domain surfaces, no clear trends (either increase or decrease) in all of those three quantities have been observed. Importantly, we believe that such behavior of a SWCNT plugging into the WW domain and forming a complex might not be rare (total 7 out of 236 in our current simulations, and much longer simulation trajectories may increase this probability). When a hydrophobic nanoparticle falls onto a particular region of a protein, where there is a match between the nanoparticle surface and the protein hydrophobic patch, such as the one between the second and third β-strands of WW domain and SWCNT, it becomes possible to have the SWCNT inserted into the protein. The strong hydrophobic interaction between the nanoparticle and the hydrophobic patch in the β-strands compensates the loss of the native contacts between the original β-strands.

In each case of a SWCNT plugging into the YAP65WW domain, we have found that the YAP65WW domain displays the same binding site after relentless search. In order to understand the mechanism behind this, we computed the root mean square fluctuations (rmsf) of the average of non-hydrogen atoms of each residue for the YAP65WW domain (Figure 4). It is clear that the loops and the turns have larger fluctuations in general. For the three β-strands, the fluctuations of the third β-strand residues are significantly higher than those of the other two β-strands. This indicates that the third β-strand is more flexible than the other two β-strands, which makes the SWCNT easier to penetrate into the domain near the third β-strand (and its neighboring β-strand, the second β-strand).

The formation of this protein−SWCNT complex may disrupt or block those key residues in the WW domain active site from their binding to the proline-rich peptides. The SWCNT insertion of the binding site is much more disruptive than the typical surface adsorption, which may result in the loss of the original function of the WW domain. To demonstrate this, we performed simulations for the system with the PRM of a sequence GTPPPPYTVG and the protein−SWCNT with its initial position 25 Å from the target. A total of 10 independent simulations, each with 200 ns, were performed (see details in Computational Methods). It was found that the YAP65WW−SWNT complex was stable in all of the simulations, and the PRM always bound to the SWCNT instead of the binding site of the YAP65WW, as one representative structure shown in Figure 1 (as a

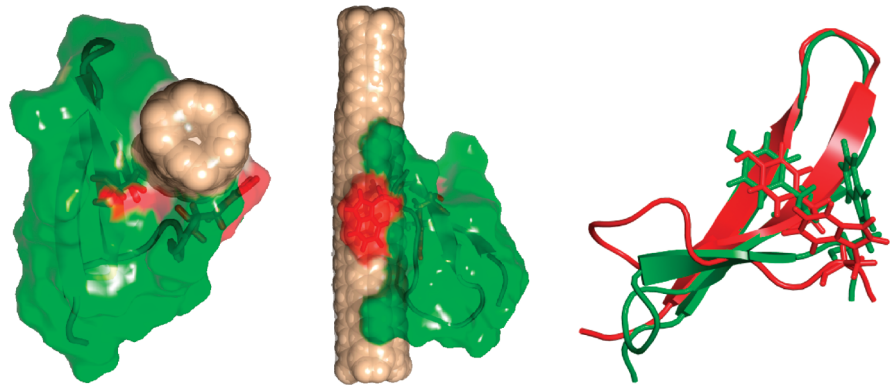

Figure 5. One representative complex structure of YAP65WW domain inserted with a longer 40 Å (4,4) SWCNT (shown in two angle views), and its comparison with the native structure (complex structure: red, native structure: green; superimposed). Here, the YAP65WW protein domain is shown as a cartoon with yellow strands and green loops, and the key residues (W39 and Y28) are identified by red sticks. The (4,4) armchair SWCNT has a diameter of 5.38 Å and a length of 40 Å, and its atoms are shown as wheat spheres. The solvated surfaces are shown for the complex.

contrast, we show the native structure that the YAP65WW domain binds the PRM in Figure 1 (bottom right)). These findings indicate that the insertion of the SWCNT indeed disabled the function of YAP65WW domain (identifying and binding the PRM) from our *in silico* approach. To validate this prediction from our *in silico* approach, *in vitro* and/or *in vivo* experiments are highly needed. Interestingly, there is recent evidence from both experiment and theory showing that some antibody from the mouse immune repertoire can "absorb" nanoparticle C_{60} through similar hydrophobic interactions.[59,60]

All of the above simulations were done with relatively short SWCNTs (~20 Å); in order to see whether longer SWCNTs might exhibit a similar behavior, we have performed additional simulations, a total of 6, with each of 200 ns, for the YAP65WW domain interacting with a (4,4) SWCNT of 40 Å in length. During these 6 trajectories, some familiar structures of the above shorter SWCNT-inserted complex structure have been observed (we name them "pre-plugging" structures). Then, 5 additional 300+ ns long simulations starting from one such pre-plugging structure have been performed further. In 2 of these 5 continuing trajectories, we have observed SWCNT inserted complex structures (*i.e.*, the SWCNT has plugged into the YAP65WW domain). Figure 5 shows one such complex structure. The complex structure is very similar to the previous shorter SWCNT-inserted complex structure (see Figure 1). Therefore, the longer SWCNTs seem to be able to insert into the WW domain core, as well, and thus disrupt the binding site associated with those key hydrophobic residues and block their binding to the proline-rich peptides. It should be noted though that the diameter of the (4,4) SWCNT is slightly smaller than that of the (6,6) SWCNT, so the "damage" to the residue W39 conformation is slightly smaller than that in the previous complex (shown in Figure 1). Nevertheless, the current simulations show that the insertion of the SWCNTs into the WW domain can happen in both 20 and 40 Å long nanotubes. It should be noted though that a recent experiment has shown that long SWCNTs can be biodegraded into very small fragments by the enzyme horseradish peroxidase (HRP),[61] thus short SWCNTs might exist and be of importance in living cells, as well. Therefore, studying SWCNTs with such relatively short lengths (20−40 Å) might be of significant importance to nanoparticle toxicity, as well.

CONCLUSION

We have found that a SWCNT plugs into the hydrophobic core of protein WW domains to form a stable protein−SWCNT complex. This results in the disrupting and blocking of PRM active sites and thus reduces the possibility of the direct binding between the PRM and the WW domain. It is the small size of the SWCNT that makes its insertion into the hydrophobic core of a protein feasible, which results in the complete disruption of the active sites. This is presumably more significant in terms of protein function "poisoning" than the mere absorption of the protein onto the nanoparticle surfaces. Consequently, the existence of the SWCNT may lead to the loss of protein function, suggesting the nanoparticle toxicity of the hydrophobic nanoparticles. Considering that the hydrophobic interaction is the main factor for the insertion of the SWCNT into the protein domain, our observation from these WW domains might indicate a common route for the interactions of other hydrophobic nanoparticles and proteins.

COMPUTATIONAL METHODS

The protein YAP65WW domain was prepared from the Protein Data Bank (PDB code 1JMQ, truncated to include residues 15−40) and modeled by AMBER03 force field.[62] All SWCNTs used in this work are armchair of (m,n), where $m = n$ = {4, 5, 6}, corresponding to the tube diameters of {5.38, 6.73, and 8.08 Å}, respectively. The lengths of all of those SWCNTs are 19.54 Å. The SWCNTs used here are shorter than the typical SWCNTs in experiment due to the extensive computational resources needed for longer SWCNTs and thus larger systems (at the end of the Results section, we also added new simulations on a longer SWCNT, with 40 Å in length; see below). The carbon atoms of the SWCNTs

were modeled as uncharged Lennard-Jones particles with a cross section of $\sigma_{cc} = 3.40$ Å and a depth of the potential well of $\varepsilon_{cc} = 0.36$ kJ/mol.[50,51] The interactions between these carbon atoms of SWCNTs and other atoms are generated by the AMBER03 force field.[62] The combined systems are then solvated in rhombic dodecahedral periodic boxes with the distance between the solutes and box boundary being at least 8 Å. The numbers of water molecules were 2694, 2709, and 2735 for the system with the SWNT of $m = 4$, 5, and 6, respectively, and a Cl^- is added into solution to neutralize the system.

The MD simulations were performed by using the Gromacs package 4.0.[63] In the simulations, the covalent bonds involving H atoms were constrained by the LINCS algorithn, allowing a time step of 2 fs. The long-range electrostatic interactions were treated with the particle-mesh Ewald method (PME) with a grid spacing of 1 Å. The cutoff for the van der Waals interaction was set to 10 Å. After energy minimization, all of the systems were equilibrated by MD simulations for 200 ps at a constant pressure of 1 bar and temperature of 298 K using Berendsen coupling. Then all simulations were performed in the NVT ensemble at 298K (and some also at 310 K; see Supporting Information). Six trajectories of 200 ns are obtained for every system with different SWCNTs.

In the PRM binding simulations, the PRM with a sequence GTPPPPYTVG was initially placed at 25 Å away from the complex of YAP65WW domain and the SWCNT. This system is again solvated in a rhombic dodecahedral periodic box with the distance between the solutes and box boundary being at least 8 Å. There are 7045 TIP3P water molecules and one Cl^-, which is used to neutralize the system. The energy minimization and the NPT MD simulation at 298 K were performed to obtain proper density. Then 10 independent simulations were performed for each system with the NVT ensemble at 298 K. Other force field and MD parameters were set the same to that of the simulation of YAP65WW domain and SWCNT above.

Acknowledgment. We thank Wenpeng Qi, Chunlei Wang, Jun Hu, Bruce Berne, Payel Das, and Peng Xiu for helpful discussions. This research is supported in part by grants from NNSFC (10825520), NBRPC (973 Program: 2007CB936000 and 2007CB814800), Shanghai Leading Academic Discipline Project (B111), and Shanghai Supercomputer Center of China. R.Z. acknowledges the support from the IBM BlueGene Science Program.

Supporting Information Available: List of all of our simulation systems, the conformational fluctuation of the YAP65WW domain at room temperature, other protein−SWCNT complexes that we have observed, and the movie of the SWCNT plug into the YAP65WW domain. This material is available free of charge *via* the Internet at http://pubs.acs.org.

REFERENCES AND NOTES

1. Rosi, N. L.; Giljohann, D. A.; Thaxton, C. S.; Lytton-Jean, A. K. R.; Han, M. S.; Mirkin, C. A. Oligonucleotide-Modified Gold Nanoparticles for Intracellular Gene Regulation. *Science* **2006**, *312*, 1027–1030.
2. Michalet, X.; Pinaud, F. F.; Bentolila, L. A.; Tsay, J. M.; Doose, S.; Li, J. J.; Sundaresan, G.; Wu, A. M.; Gambhir, S. S.; Weiss, S. Quantum Dots for Live Cells, *In Vivo* Imaging, and Diagnostics. *Science* **2005**, *307*, 538–544.
3. Wang, X.; Yang, L. L.; Chen, Z.; Shin, D. M. Application of Nanotechnology in Cancer Therapy and Imaging. *CA Cancer J. Clin.* **2008**, *58*, 97–110.
4. Li, H. K.; Huang, J. H.; Lv, J. H.; An, H. J.; Zhang, X. D.; Zhang, Z. Z.; Fan, C. H.; Hu, J. Nanoparticle PCR: Nanogold-Assisted PCR with Enhanced Specificity. *Angew. Chem., Int. Ed.* **2005**, *44*, 5100–5103.
5. Service, R. F. Is Nanotechnology Dangerous? *Science* **2000**, *290*, 1526–1527.
6. Donaldson, K.; Aitken, R.; Tran, L.; Stone, V.; Duffin, R.; Forrest, G.; Alexander, A. Carbon Nanotubes: A Review of Their Properties in Relation to Pulmonary Toxicology and Workplace Safety. *Toxicol. Sci.* **2006**, *92*, 5–22.
7. Gilbert, N. Nanoparticle Safety in Doubt. *Nature* **2009**, *460*, 937.
8. Nel, A.; Xia, T.; Madler, L.; Li, N. Toxic Potential of Materials at the Nanolevel. *Science* **2006**, *311*, 622–627.
9. Zhao, Y. L.; Xing, G. M.; Chai, Z. F. Nanotoxicology: Are Carbon Nanotubes Safe? *Nat. Nanotechnol.* **2008**, *3*, 191–192.
10. Chen, Z.; Meng, H.; Xing, G. M.; Chen, C. Y.; Zhao, Y. L.; Jia, G.; Wang, T. C.; Yuan, H.; Ye, C.; Zhao, F.; *et al.* Acute Toxicological Effects of Copper Nanoparticles *In Vivo*. *Toxical. Lett.* **2006**, *163*, 109–120.
11. Maynard, A. D.; Baron, P. A.; Foley, M.; Shvedova, A. A.; Kisin, E. R.; Castranova, V. Exposure to Carbon Nanotube Material: Aerosol Release During the Handling of Unrefined Single-Walled Carbon Nanotube Material. *J. Toxicol. Environ. Health A* **2004**, *67*, 87–107.
12. Ryman-Rasmussen, J. P.; Cesta, M. F.; Brody, A. R.; Shipley-Phillips, J. K.; Everitt, J. I.; Tewksbury, E. W.; Moss, O. R.; Wong, B. A.; Dodd, D. E.; Andersen, M. E.; *et al.* Inhaled Carbon Nanotubes Reach the Subpleural Tissue in Mice. *Nat. Nanotechnol.* **2009**, *4*, 747–751.
13. Kolosnjaj, J.; Szwarc, H.; Moussa, F. Toxicity Studies of Carbon Nanotubes. *Adv. Exp. Med. Biol.* **2007**, *620*, 181–204.
14. Porter, A. E.; Gass, M.; Muller, K.; Skepper, J. N.; Midgley, P. A.; Welland, M. Direct Imaging of Single-Walled Carbon Nanotubes in Cells. *Nat. Nanotechnol.* **2007**, *2*, 713–717.
15. Ma-Hock, L.; Treumann, S.; Strauss, V.; Brill, S.; Luizi, F.; Mertler, M.; Wiench, K.; Gamer, A. O.; van Ravenzwaay, B.; Landsiedel, R. Inhalation Toxicity of Multiwall Carbon Nanotubes in Rats Exposed for 3 Months. *Toxicol. Sci.* **2009**, *112*, 468–481.
16. Poland, C. A.; Duffin, R.; Kinloch, I.; Maynard, A.; Wallace, W. A. H.; Seaton, A.; Stone, V.; Brown, S.; MacNee, W.; Donaldson, K. Carbon Nanotubes Introduced into the Abdominal Cavity of Mice Show Asbestos-like Pathogenicity in a Pilot Study. *Nat. Nanotechnol.* **2008**, *3*, 423–428.
17. Schipper, M. L.; Nakayama-Ratchford, N.; Davis, C. R.; Kam, N. W. S.; Chu, P.; Liu, Z.; Sun, X. M.; Dai, H. J.; Gambhir, S. S. A Pilot Toxicology Study of Single-Walled Carbon Nanotubes in a Small Sample of Mice. *Nat. Nanotechnol.* **2008**, *3*, 216–221.
18. Shvedova, A. A.; Kisin, E. R.; Mercer, R.; Murray, A. R.; Johnson, V. J.; Potapovich, A. I.; Tyurina, Y. Y.; Gorelik, O.; Arepalli, S.; Schwegler-Berry, D.; *et al.* Unusual Inflammatory and Fibrogenic Pulmonary Responses to Single-Walled Carbon Nanotubes in Mice. *Am. J. Physiol. Lung Cell. Mol. Physiol.* **2005**, *289*, L698–L708.
19. Mitchell, L. A.; Lauer, F. T.; Burchiel, S. W.; McDonald, J. D. Mechanisms for How Inhaled Multiwalled Carbon Nanotubes Suppress Systemic Immune Function in Mice. *Nat. Nanotechnol.* **2009**, *4*, 451–456.
20. Li, Z.; Hulderman, T.; Salmen, R.; Chapman, R.; Leonard, S. S.; Young, S.-H.; Shvedova, A.; Luster, M. I.; Simeonova, P. P. Cardiovascular Effects of Pulmonary Exposure to Single-Wall Carbon Nanotubes. *Environ. Health Perspect.* **2007**, *115*, 377–382.
21. Cedervall, T.; Lynch, I.; Lindman, S.; Berggård, T.; Thulin, E.; Nilsson, H.; Dawson, K. A.; Linse, S. Understanding the Nanoparticle−Protein Corona Using Methods to Quantify Exchange Rates and Affinities of Proteins for Nanoparticles. *Proc. Natl. Acad. Sci. U.S.A.* **2007**, *104*, 2050–2055.
22. Klein, J. Probing the Interactions of Proteins and Nanoparticles. *Proc. Natl. Acad. Sci. U.S.A.* **2007**, *104*, 2029–2030.
23. Rocker, C.; Potzl, M.; Zhang, F.; Parak, W. J.; Nienhaus, G. U. A Quantitative Fluorescence Study of Protein Monolayer Formation on Colloidal Nanoparticles. *Nat. Nanotechnol.* **2009**, *4*, 577–580.
24. Shen, J. W.; Wu, T.; Wang, Q.; Kang, Y. Induced Stepwise Conformational Change of Human Serum Albumin on Carbon Nanotube Surfaces. *Biomaterials* **2008**, *29*, 3847–3855.

25. Xiao, Y.; Patolsky, F.; Katz, E.; Hainfeld, J. F.; Willner, I. "Plugging into Enzymes": Nanowiring of Redox Enzymes by a Gold Nanoparticle. *Science* **2003**, *299*, 1877–1881.
26. Saven, J. G. Computational Protein Design: Advances in the Design and Redesign of Biomolecular Nanostructures. *Curr. Opin. Colloid Interface Sci.* **2010**, *15*, 13–17.
27. Kang, Y.; Wang, Q.; Liu, Y. C.; Wu, T.; Chen, Q.; Guan, W. J. Dynamic Mechanism of Collagen-like Peptide Encapsulated into Carbon Nanotubes. *J. Phys. Chem. B* **2008**, *112*, 4801–4807.
28. Park, K. H.; Chhowalla, M.; Iqbal, Z.; Sesti, F. Single-Walled Carbon Nanotubes Are a New Class of Ion Channel Blockers. *J. Biol. Chem.* **2003**, *278*, 50212–50216.
29. Calvaresi, M.; Zerbetto, F. Baiting Proteins with C-60. *ACS Nano* **2010**, *4*, 2283–2299.
30. Macias, M. J.; Hyvonen, M.; Baraldi, E.; Schultz, J.; Sudol, M.; Saraste, M.; Oschkinat, H. Structure of the WW Domain of a Kinase-Associated Protein Complexed with a Proline-Rich Peptide. *Nature* **1996**, *382*, 646–649.
31. Iijima, S. Helical Microtubules of Graphitic Carbon. *Nature* **1991**, *354*, 56–58.
32. Li, W. Z.; Xie, S. S.; Qian, L. X.; Chang, B. H.; Zou, B. S.; Zhou, W. Y.; Zhao, R. A.; Wang, G. Large-Scale Synthesis of Aligned Carbon Nanotubes. *Science* **1996**, *274*, 1701–1703.
33. Duan, Y.; Kollman, P. A. Pathways to a Protein Folding Intermediate Observed in a 1-Microsecond Simulation in Aqueous Solution. *Science* **1998**, *282*, 740–744.
34. Levy, Y.; Wolynes, P. G.; Onuchic, J. N. Protein Topology Determines Binding Mechanism. *Proc. Natl. Acad. Sci. U.S.A.* **2004**, *101*, 511–516.
35. Snow, C. D.; Nguyen, H.; Pande, V. S.; Gruebele, M. Absolute Comparison of Simulated and Experimental Protein-Folding Dynamics. *Nature* **2002**, *420*, 102–106.
36. Zhou, R. H.; Huang, X. H.; Margulis, C. J.; Berne, B. J. Hydrophobic Collapse in Multidomain Protein Folding. *Science* **2004**, *305*, 1605–1609.
37. Liu, P.; Huang, X. H.; Zhou, R. H.; Berne, B. J. Observation of a Dewetting Transition in the Collapse of the Melittin Tetramer. *Nature* **2005**, *437*, 159–162.
38. Zuo, G. H.; Hu, J.; Fang, H. P. Effect of the Ordered Water on Protein Folding: An Off-Lattice Gō-Like Model Study. *Phys. Rev. E* **2009**, *79*, 031925.
39. Mayor, U.; Guydosh, N. R.; Johnson, C. M.; Grossmann, J. G.; Sato, S.; Jas, G. S.; Freund, S. M. V.; Alonso, D. O. V.; Daggett, V.; Fersht, A. R. The Complete Folding Pathway of a Protein from Nanoseconds to Microseconds. *Nature* **2003**, *421*, 863–867.
40. Mirny, L.; Shakhnovich, E. Protein Folding Theory: From Lattice to All-Atom Models. *Annu. Rev. Biophys. Biomol. Struct.* **2001**, *30*, 361–396.
41. Garcia, A. E.; Paschek, D. Simulation of the Pressure and Temperature Folding/Unfolding Equilibrium of a Small RNA Hairpin. *J. Am. Chem. Soc.* **2008**, *130*, 815–816.
42. Miyashita, N.; Straub, J. E.; Thirumalai, D. Structures of β-Amyloid Peptide 1−40, 1−42, and 1−55-the 672−726 Fragment of App in a Membrane Environment with Implications for Interactions with γ-Secretase. *J. Am. Chem. Soc.* **2009**, *131*, 17843–17852.
43. Hua, L.; Huang, X.; Zhou, R.; Berne, B. J. Dynamics of Water Confined in the Interdomain Region of a Multidomain Protein. *J. Phys. Chem. B* **2006**, *110*, 3704–3711.
44. Liu, P.; Huang, X.; Zhou, R.; Berne, B. J. Hydrophobic Aided Replica Exchange: An Efficient Algorithm for Protein Folding in Explicit Solvent. *J. Phys. Chem. B* **2006**, *110*, 19018–19022.
45. Zhou, R. Exploring the Protein Folding Free Energy Landscape: Coupling Replica Exchange Method with P3me/Respa Algorithm. *J. Mol. Graphics Modell.* **2004**, *22*, 451–463.
46. Zhou, R.; Eleftheriou, M.; Royyuru, A. K.; Berne, B. J. Destruction of Long-Range Interactions by a Single Mutation in Lysozyme. *Proc. Natl. Acad. Sci. U.S.A.* **2007**, *104*, 5824–5829.
47. Gao, Y. Q.; Yang, W.; Karplus, M. A Structure-Based Model for the Synthesis and Hydrolysis of ATP by F1-Atpase. *Cell* **2005**, *123*, 195–205.
48. Karplus, M.; Gao, Y. Q.; Ma, J.; van der Vaart, A.; Yang, W. Protein Structural Transitions and Their Functional Role. *Philos. Trans. R. Soc., A* **2005**, *363*, 331–355; discussion 355−356.
49. Roitberg, A. E.; Okur, A.; Simmerling, C. Coupling of Replica Exchange Simulations to a Non-Boltzmann Structure Reservoir. *J. Phys. Chem. B* **2007**, *111*, 2415–2418.
50. Gong, X. J.; Li, J. Y.; Lu, H. J.; Wan, R. Z.; Li, J. C.; Hu, J.; Fang, H. P. A Charge-Driven Molecular Water Pump. *Nat. Nanotechnol.* **2007**, *2*, 709–712.
51. Hummer, G.; Rasaiah, J. C.; Noworyta, J. P. Water Conduction through the Hydrophobic Channel of a Carbon Nanotube. *Nature* **2001**, *414*, 188–190.
52. Tu, Y. S.; Xiu, P.; Wan, R. Z.; Hu, J.; Zhou, R. H.; Fang, H. P. Water-Mediated Signal Multiplication with Y-Shaped Carbon Nanotubes. *Proc. Natl. Acad. Sci. U.S.A.* **2009**, *106*, 18120–18124.
53. Li, J. Y.; Gong, X. J.; Lu, H. J.; Li, D.; Fang, H. P.; Zhou, R. H. Electrostatic Gating of a Nanometer Water Channel. *Proc. Natl. Acad. Sci. U.S.A.* **2007**, *104*, 3687–3692.
54. Giovambattista, N.; Lopez, C. F.; Rossky, P. J.; Debenedetti, P. G. Hydrophobicity of Protein Surfaces: Separating Geometry from Chemistry. *Proc. Natl. Acad. Sci. U.S.A.* **2008**, *105*, 2274–2279.
55. Dill, K. Dominant Forces in Protein Folding. *Biochemistry* **1990**, *29*, 7133–7155.
56. Wang, S.; Humphreys, E. S.; Chung, S. Y.; Delduco, D. F.; Lustig, S. R.; Wang, H.; Parker, K. N.; Rizzo, N. W.; Subramoney, S.; Chiang, Y. M.; Jagota, A. Peptides with Selective Affinity for Carbon Nanotubes. *Nat. Mater.* **2003**, *2*, 196–200.
57. Zheng, L. F.; Jain, D.; Burke, P. Nanotube−Peptide Interactions on a Silicon Chip. *J. Phys. Chem. C* **2009**, *113*, 3978–3985.
58. Kabsch, W.; Sander, C. Dictionary of Protein Secondary Structure: Pattern Recognition of Hydrogen-Bonded and Geometrical Features. *Biopolymers* **1983**, *22*, 2577–2637.
59. Braden, B. C.; Goldbaum, F. A.; Chen, B. X.; Kirschner, A. N.; Wilson, S. R.; Erlanger, B. F. X-ray Crystal Structure of an Anti-Buckminsterfullerene Antibody Fab Fragment: Biomolecular Recognition of C(60). *Proc. Natl. Acad. Sci. U.S.A.* **2000**, *97*, 12193–12197.
60. Noon, W. H.; Kong, Y.; Ma, J. Molecular Dynamics Analysis of a Buckyball−Antibody Complex. *Proc. Natl. Acad. Sci. U.S.A.* **2002**, *99*, 6466–6470.
61. Allen, B. L.; Kichambare, P. D.; Gou, P.; Vlasova, I. I.; Kapralov, A. A.; Konduru, N.; Kagan, V. E.; Star, A. Biodegradation of Single-Walled Carbon Nanotubes through Enzymatic Catalysis. *Nano Lett.* **2008**, *8*, 3899–2903.
62. Duan, Y.; Wu, C.; Chowdhury, S.; Lee, M. C.; Xiong, G. M.; Zhang, W.; Yang, R.; Cieplak, P.; Luo, R.; Lee, T. S.; *et al.* A Point-Charge Force Field for Molecular Mechanics Simulations of Proteins Based on Condensed-Phase Quantum Mechanical Calculations. *J. Comput. Chem.* **2003**, *24*, 1999–2012.
63. Hess, B.; Kutzner, C.; van der Spoel, D.; Lindahl, E. Gromacs 4: Algorithms for Highly Efficient, Load-Balanced, and Scalable Molecular Simulation. *J. Chem. Theory Comp.* **2008**, *4*, 435–447.